High Strength, Molecularly Thin Nanoparticle Membranes

K. Michael Salerno, Dan S. Bolintineanu, J. Matthew D. Lane, and Gary S. Grest

Phys. Rev. Lett. **113**, 258301 — Published 17 December 2014

DOI: 10.1103/PhysRevLett.113.258301

High strength, molecularly thin nanoparticle membranes

K. Michael Salerno,[1,*] Dan S. Bolintineanu,[1] J. Matthew D. Lane,[1] and Gary S. Grest[1]

[1] *Sandia National Laboratories, Albuquerque, NM, 87185*

The unique strength observed in molecular thin films consisting of assemblies of nanoparticles encoded with short organic chains opens an intriguing new realm of controllable materials. Here the fundamental mechanisms underlying this unique mechanical strength are probed by molecular dynamics simulations. Using nanoparticles encoded with short hydrocarbon chains, we show that the mechanical response and failure of single nanoparticle thick membranes depend on subtle changes of the coating. Extremely high moduli were observed in agreement with experiment. We calculate the Young's modulus for the membrane system based on properties of the individual components and find that ligand end-group interactions explain the observed changes in mechanical properties. Specifically, for dodecanethiol chains on 6 nm diameter gold cores, the Young's modulus is 2.5 GPa for CH_3 terminated chains and increases by 50% when end groups are replaced by COOH.

Recent experimental studies of nanometer thick membranes formed from a single layer of nanoparticles (NPs) encoded with short organic chains found that they are surprisingly strong despite their nanoscale dimension [1–3]. Freestanding, two-dimensional NP membranes have been found to have remarkably large mechanical stiffness, with Young's moduli on the order 1-10 GPa [1, 3, 4], even though membranes contain no crosslinks. Due to their unusual strength, these thin membranes have a number of potential applications from sensor arrays to nanoscale filtration [5, 6]. The stiffness of the membrane, as reflected in elastic moduli, varies with the length and composition of the encoded ligands. While both the ligand-NP binding strength and the ligand-ligand interaction have been found to play a role in determining membrane mechanical properties [1], the underlying microscopic origin of the strength of these membranes remains unresolved.

Experimentally, single NP membranes have been formed in a variety of ways, including using evaporation induced ordering [3, 7] and DNA-programmable NPs [8]. In the case of evaporation induced ordering, NPs are driven by evaporation to the liquid/vapor interface [7]. As evaporation proceeds, the reduction in surface area of the liquid/vapor interface and NP attraction drive aggregation and membrane formation. After drying, membranes are supported on a silicon-nitride substrate with micrometer size holes cut in the substrate to test the mechanical response of the freestanding membrane. Membrane mechanical properties can be probed using resonance frequency, bulge, and atomic force microscopy (AFM) indentation tests [2, 4].

Here the fundamental mechanisms underlying the unique mechanical strength of these single NP thick membranes are probed by molecular dynamics (MD) simulations. We show how the mechanical response and failure of single NP thick membranes depend on subtle features of the coating. Our fully atomistic MD simulations of membranes composed of alkanethiol-coated gold NPs provide a nanoscale picture of ligand interactions and structure that cannot easily be obtained experimentally. Multi-million atom simulations of NP membranes like those shown in Fig. 1(a) allow us to simultaneously measure nanoscale interactions while directly comparing membrane properties with those found experimentally [1, 2, 9]. Our simulations show that the interactions between end-groups on the encoded ligands play a dominant role in determining membrane strength and stiffness. An estimate of the end-group contribution to membrane stiffness indicates that these interactions account for the observed changes in stiffness.

There have been a limited number of simulation studies of the aggregation and assembly of NPs. Early simulations of mechanical properties of three-dimensional Au NP assemblies were carried out by Luedtke and Landman [10, 11]. More recently, Ngo *et al.* [12] examined the mechanical properties of three-dimensional crystals of DNA-functionalized NPs. Both studies found crystalline NP structures with elastic moduli on the order of 1 GPa. At the liquid/vapor interface the aggregation of encoded NPs were studied by Lane and Grest [13] and Lin *et al.* [14].

Here we study 6nm Au NP with S-$(CH_2)_{11}$X alkanethiol ligands, where X is either carboxylic acid (COOH) or methyl (CH_3). The system was chosen since for X=CH_3 we can directly compare our results for Young's modulus with those of He *et al.* [1]. The preparation of the NPs follows the procedure outlined in [15] with some modification [16]. Here the Au NP core is explicitly modeled to capture the heterogeneity in the sulfur binding locations and to account for Au-ligand interactions. Initially the 6 nm gold core is explicitly simulated with an embedded atom model (EAM) potential[17] to model softening of the edges and facets of the nanocrystal. Next, a vapor of sulfur atoms is allowed to deposit and bind to the gold surface. Gold-sulfur Lennard-Jones parameters are selected to produce an adsorbed sulfur surface density of $4.7\,/\mathrm{nm}^2$, consistent with experiment [18]. During this process the Au surface is able to relax to accommodate the adsobred sulfur. Experimentally upon physisorption, the alkanethiol molecule binds to the Au nanoparticle through the sulfur atom and loses the mercaptan H atom, transforming itself into an alkanethiolate

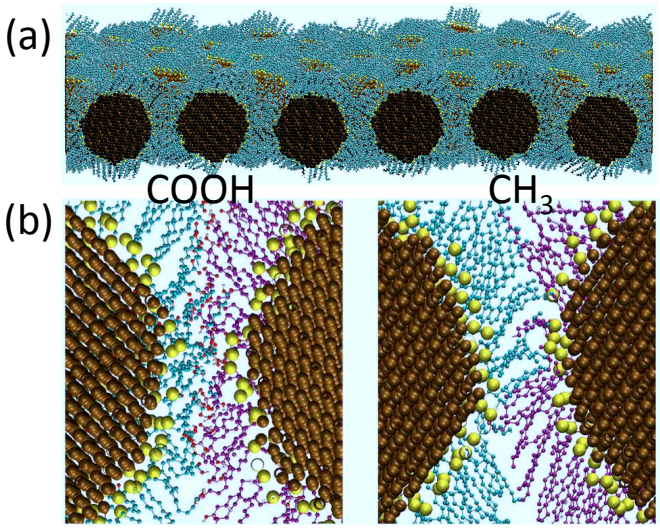

FIG. 1. (a) (Color online) Angled side view of CH_3-terminated dry membrane prior to deformation. Hydrogen atoms are represented in white, carbon in cyan, gold in brown, and sulfur in yellow. (b) A close-up view of COOH terminated (left) and CH_3-terminated (right) NPs in a dry membrane prior to deformation. Hydrogen atoms have been omitted except in the COOH end group. In both cases carbon atoms on the left NP are colored cyan while those on the right are colored purple.

[19]. Initially chains are in the all-trans configuration and bonded to the deposited sulfur atoms. Ligand interactions are modeled using the OPLS-AA force field [20], and water molecules are simulated using the TIP4P/2005 model [21, 22] with angles constrained via the SHAKE algorithm [23]. The gold and sulfur atoms comprising the NP core are treated as a rigid body after the initial simulations to determine the surface binding sites.

In order to form a membrane a two-dimensional 6×6 hexagonal NP array was initially placed atop a $60.0 \times 51.96 \times 8.0\,\mathrm{nm}^3$ water slab. Throughout the membrane formation process a Langevin thermostat with time constant 1 ps was applied to both ligand and water molecules to control the temperature [24]. Including fully outstretched ligands, the NPs have a 8 nm to 9 nm diameter, and the initial NP spacing $a_0 = 10.0\,\mathrm{nm}$ was chosen so that NPs are not touching. The simulation cell is periodic in all three directions, with size L_z =30.0 nm in the z-direction, allowing for ample space between the NPs and the periodic image of the water-vapor interface. Nanoparticles were placed at the interface rather than in the bulk because migration of the NPs from the bulk to the interface is a slow process.

Starting from the initial 10.0 nm lattice spacing, we compressed the membrane isotropically over 0.4 ns. As the final state is known to be hexagonal from experiment, the NP cores are constrained to their lattice positions during compression. They move only due to the applied strain and do not experience forces from other atoms. States for mechanical testing were chosen to have NP lattice constant of 7.53 nm for both the CH_3 and COOH samples. These spacings are the middle of a range over which the mechanical properties are independent of lattice spacing. The values agree with experimental lattice spacings of 7.4 nm for CH_3-terminated chains on 6 nm gold NPs [2].

After compression, NP membranes were equilibrated for 0.2 ns at the water-vapor interface with no constraints on the NP cores. The water was then removed, leaving a dry, freestanding membrane. An example of an undeformed freestanding membrane with CH_3 end groups is shown in Fig. 1(a). Finally, the dry membrane was equilibrated for a period of 0.2 ns to 10 ns. Longer equilibration periods were used to check that membrane properties are independent of equilibration time. Over 10 ns the COOH membrane showed a small increase in stiffness, within the measurement error.

Figure 1(b) shows close-up views of two NPs from the COOH and CH_3 membranes. It can be seen from the figure that there is some interdigitation, but there are also many ligands oriented to splay out of the volume between the NP surfaces. Ligands from neighboring NPs are far from fully interpenetrated. The packing of ligands that leads to the lack of interdigitation strongly resembles that seen in NPs displaying spontaneous asymmetry [13]. The COOH ligands tend to pack and splay less, but instead bend to keep end groups from neighboring NPs close to one another.

For both the COOH and CH_3 terminated ligands shown in Fig. 1(b) interdigitation appears minor, with packed ligand regions that splay or bend rather than fully interpenetrating. This modifies the picture of full ligand interdigitation used previously to explain NP spacing of 7.4 nm in experiments [1]. Below, we report that elastic moduli of our membranes are comparable to those measured experimentally, indicating that a fully interdigitated ligand geometry is not necessary for mechanical stability. Furthermore, the COOH membrane, which shows less interdigitation than the CH_3 membrane, shows increased stiffness. These facts indicate that the electrostatic interactions of end-groups can be important to ligand structure and membrane properties, and must be treated along with van der Waals interactions in considering membrane properties.

Following the water removal, the freestanding membrane was subjected to a number of deformations to measure its mechanical properties. For some simulations, the membrane was replicated in the x or y directions (or both) in order to test for finite size effects. For certain simulations the membrane was also "unwrapped" around the periodic boundary conditions in order to test the effects of periodic boundaries on the mechanical properties. In this case, NPs spanning the periodic boundary in the "open" direction were assigned to one side of the box and the box was expanded by 3.0 nm on each side of the

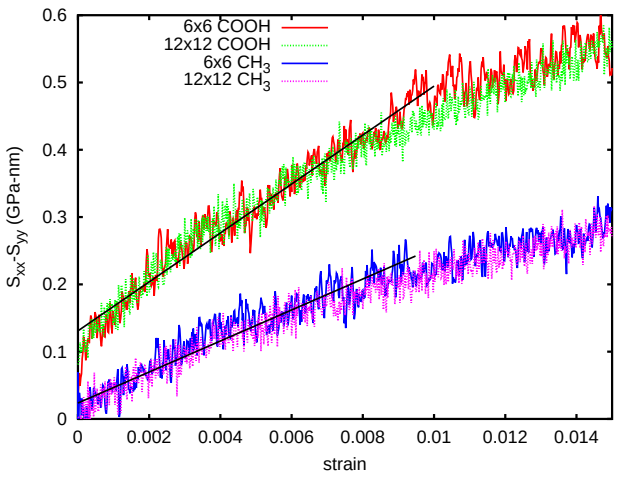

FIG. 2. (Color online) Typical two-dimensional stress-strain curves for samples undergoing pure shear deformation. Data have been time averaged over 0.4 ps, and curves for the 6x6 membranes have been further smoothed as described in the text. The COOH terminated NP membrane shows a stiffer characteristic response than the CH_3 membrane.

membrane.

Mechanical properties of the freestanding membranes were measured by performing extension and compression in a single direction or both directions, as well as pure shear simulations. Samples were deformed by affinely deforming the ligands and affinely displacing the NP cores to match the strain imposed on the simulation box. Strain rates $\dot{\epsilon} = 5 \times 10^7 s^{-1}$ corresponding to maximum velocities of about 3 m/s were used.

Figure 2 shows a two-dimensional stress-strain curve from membranes undergoing pure shear. During this test samples undergo extension in the y-direction and compression in the x-direction while preserving the total area. Membranes of size 6×6 and 12×12 NPs are compared, showing no finite size effects. Data for all systems have been averaged over a 0.4 ps interval and data for smaller membranes have been further smoothed to reduce noise. The fit to the initial linear elastic portion is shown, and the two-dimensional shear modulus μ^{2D} may be read from the plot as 1/4 the slope of the two-dimensional stress-strain curve. Measurements of stresses and elastic constants are two-dimensional, with units of GPa-nm, and are independent of sample thickness. To compare with reported three-dimensional moduli we divide the 2D moduli by the sample thickness 7.5 ± 0.3nm [1].

The COOH and CH_3 systems shown in Fig. 2 are comparable to those measured in experiment. The COOH sample has a Young's modulus of $E = 3.7 \pm 0.4$ GPa, while the CH_3 sample is less stiff with $E = 2.5 \pm 0.4$ GPa. This difference in stiffness is reflected in Fig. 2. Estimates of the error of the measurement reflect the elastic constants measured with different deformation protocols. These values are of the same order as corresponding values for experimental membranes, where the average Young's modulus measured for Au NPs with CH_3-terminated ligands is 4 GPa [1]. There, values from 1 GPa to 14 GPa were measured for different samples.

We have executed a variety of simulations to verify that our simulation methodology does not influence mechanical properties. By holding a membrane at a fixed applied strain for some time before measuring the stress, we observe no viscous response in the membranes. Strain rates from $\dot{\epsilon} = 5 \times 10^6 s^{-1}$ to $\dot{\epsilon} = 5 \times 10^8 s^{-1}$ were used for a subset of simulations to check strain-rate dependence. Results for different strain rates are within the measurement error. Elastic constants measured using different applied strains, system sizes and boundary conditions vary by 10-15%.

The significantly higher Young's modulus for membranes with COOH-terminated ligands suggests that ligand end group can influence mechanical properties. One important difference between the methyl and carboxyl end groups is their electrostatic interactions. These interactions have been shown to be important in forming 3D NP structures with unique properties [25]. Charge separation between the oxygen and hydrogen atoms can lead to hydrogen bonding between COOH groups, e.g. dimers of carboxylic acid, and this feature may be important in interactions between ligands with COOH end-groups.

The affinity among end-groups is quantified by measuring the typical distance between end-group carbon atoms on neighboring NPs. We expect that an attractive interaction between end groups results in an increase in end-group carbon density at small separations. The radial density function $\rho(r)$ is calculated by forming a histogram of the distance r between an end-group carbon on one NP and the end-group carbons on all other NPs. A comparison of $\rho(r)$ for COOH and CH_3 membranes is shown in Fig. 3.

The most striking feature in Fig. 3 is the contrast in the peak height for the two different end groups. The peak in the COOH data at 0.25 nm indicates that COOH end groups from neighboring NPs are found adjacent to one another. This is likely due to electrostatic interactions between partial charges on oxygen and hydrogen atoms. This is consistent with and reinforces the observation from Fig. 1 that COOH ligands orient end-to-end. The inset in Fig. 3 shows the interface between NP ligands as represented by end-group atoms. Oxygen atoms from COOH end groups (red, left) and carbon atoms from CH_3 end-groups (cyan, right) within a 5 nm window of the mean NP height are shown. The oxygen atoms show a well-defined hexagonal cell, reiterating that ligands orient end-to-end. The CH_3 end groups show thicker, more rounded interfaces reiterating the idea demonstrated by $\rho(r)$, that the CH_3 end-groups do not show a strong affinity for one another.

Based on the affinity of the COOH end groups we make

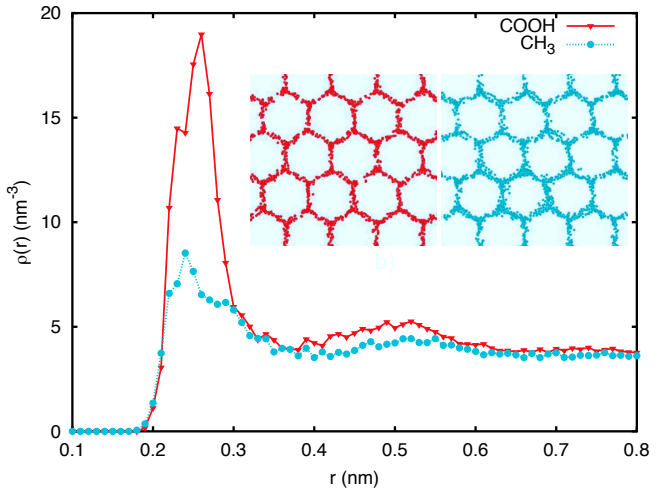

FIG. 3. (Color online) The radial density function $\rho(r)$ measures the density of end-group carbon atoms from neighboring NPs as a function of carbon-carbon separation r, contrasting the behavior for CH_3 and COOH terminated ligands. (inset) Top view of membranes showing oxygen atoms from COOH end groups (red, left) or carbon atoms from CH_3 (cyan, right) within a 5 nm slice centered at the average NP height.

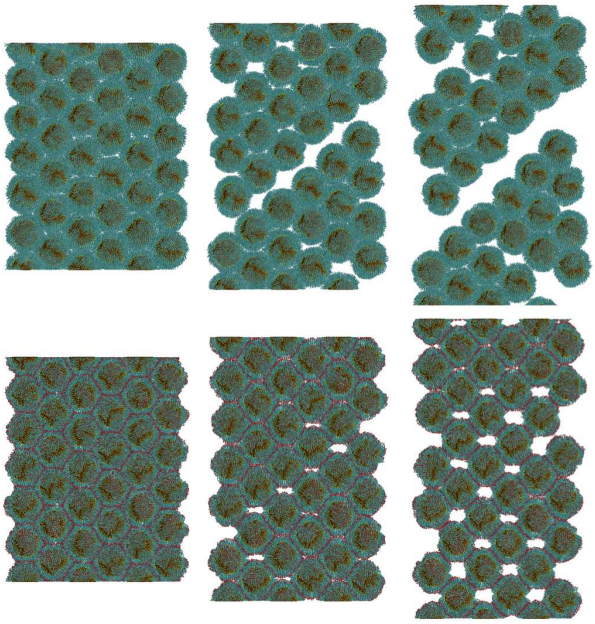

FIG. 4. (Color online) CH_3 (top) and COOH (bottom) terminated samples shown at (from left to right) 10%, 26%, and 40% strain. Failure in the CH_3 sample begins at about 26% strain. At this strain the COOH sample exhibits only void formation, and does not begin to tear until ≈40% strain. The boundary in the lateral direction is open.

an order-of-magnitude estimate of their contribution to the membrane modulus. We treat the COOH end groups as dipoles with a binding energy of 60-80 kJ/mol [25, 26] and estimate from Fig. 3 that the interactions are important for radii smaller than 0.5-0.6nm. This gives an additional contribution of 700 MPa to 800 MPa to the modulus of the ligand-ligand interface, in rough agreement with the measured modulus change. The exact value of the contribution depends on the ligand-ligand interface geometry and the ligand volume fraction, but this estimate shows that end-group interactions can have a large impact on the membrane modulus.

Failure in samples with different end groups also occurs in a different manner and at different strains. Figure 4 shows COOH and CH_3 terminated NP membranes at 10%, 26%, and 40% strain. Samples have open boundaries in the lateral direction to allow for tearing. At 26% strain the CH_3 membrane has a visible break across the membrane. In contrast, the COOH membrane has an interesting structure where elongation of ligands in the tensile direction allows the membrane to stretch and form voids. In fact, the first separation of diagonal neighbors in the COOH membrane occurs at about 40% strain. In the CH_3 sample this occurs at 24-26% strain.

In conclusion, we have shown through fully-atomistic MD simulations that experimentally measured mechanical properties of ligand-coated NP membranes can be reproduced and tied directly to nanoscale dynamics and structure. We verify that membranes with 2D hexagonal symmetry are stable and have lattice spacings consistent with experiment. Moreover, we identified molecular-scale differences in aggregate structure, which arise purely from varying ligand termination groups. Contrary to prior assumption, we show that interdigitation of encoded ligands from adjacent particles is not pervasive, and therefore is unlikely to be the principle driver of the unexpectedly large stiffness in these membranes.

Elastic moduli measured from freestanding NP membranes are in quantitative agreement with measurements from comparable experimental systems. Membranes with COOH terminated ligands demonstrate significantly higher Young's modulus and less ligand interdigitation than comparable CH_3 terminated ligand membranes. We postulate that local electrostatic interactions are responsible for the increased modulus. From molecular observation, we note an end-to-end configuration of ligands from neighboring NPs in the COOH system, which can be attributed to the electrostatic attraction between partial charges in adjacent COOH end groups. An estimate of COOH contributions indicates that the change in membrane modulus is attributable to end-group interactions. Thus, our simulations indicate that end-group interactions can significantly change nanoscale ligand behavior and can be as or more important than ligand interdigitation in determining membrane mechanical properties.

ACKNOWLEDGEMENTS

We thank X.-M. Lin and H. Jaeger for helpful discussions. This research used resources obtained through the Advanced Scientific Computing Research (ASCR) Leadership Computing Challenge (ALCC) at the National Energy Research Scientific Computing Center (NERSC), which is supported by the Office of Science of the United States Department of Energy under Contract No. DE-AC02-05CH11231. Research was carried out in part, at the Center for Integrated Nanotechnologies, a U.S. Department of Energy, Office of Basic Energy Sciences user facility. Sandia National Laboratories is a multi-program laboratory managed and operated by Sandia Corporation, a wholly owned subsidiary of Lockheed Martin Corporation, for the U.S. Department of Energy's National Nuclear Security Administration under contract DE-AC04-94AL85000.

* kmsaler@sandia.gov

[1] J. He, P. Kanjanaboos, N. L. Frazer, A. Weis, X.-M. Lin, and H. M. Jaeger, Small **6**, 1449 (2010).

[2] K. E. Mueggenburg, X.-M. Lin, R. H. Goldsmith, and H. M. Jaeger, Nat. Mater. **6**, 656 (2007).

[3] W. Cheng, M. J. Campolongo, J. J. Cha, S. J. Tan, C. C. Umbach, D. A. Muller, and D. Luo, Nat. Mater. **8**, 519 (2009).

[4] S. Markutsya, C. Jiang, Y. Pikus, and V. Tsukruk, Adv. Func. Mater. **15**, 771 (2005).

[5] C. Jiang, S. Markutsya, Y. Pikus, and V. V. Tsukruk, Nat. Mater. **3**, 721 (2004).

[6] C. C. Striemer, T. R. Gaborski, J. L. McGrath, and P. M. Fauchet, Nature **445**, 749 (2007).

[7] T. P. Bigioni, X.-M. Lin, T. T. Nguyen, E. I. Corwin, T. A. Witten, and H. M. Jaeger, Nat. Mater. **5**, 265 (2006).

[8] S. Srivastava, D. Nykypanchuk, M. Fukuto, J. D. Halverson, A. V. Tkachenko, K. G. Yager, and O. Gang, J. Am. Chem. Soc. **136**, 8323 (2014).

[9] Y. Wang, P. Kanjanaboos, E. Barry, S. Mcbride, X.-M. Lin, and H. M. Jaeger, Nano Letters **14**, 826 (2014).

[10] W. D. Luedtke and U. Landman, J. Phys. Chem. **100**, 13323 (1996).

[11] W. D. Luedtke and U. Landman, J. Phys. Chem. B **102**, 6566 (1998).

[12] V. A. Ngo, R. K. Kalia, A. Nakano, and P. Vashishta, J. Phys. Chem. C **116**, 19579 (2012).

[13] J. M. D. Lane and G. S. Grest, Nanoscale **6**, 5132 (2014).

[14] J.-Q. Lin, H.-W. Zhang, Z. Chen, Y.-G. Zheng, Z.-Q. Zhang, and H.-F. Ye, J. Phys. Chem. C **115**, 18991 (2011).

[15] J. M. D. Lane and G. S. Grest, Phys. Rev. Lett. **104**, 235501 (2010).

[16] See Supplemental Material [URL], which includes Refs. [27, 28].

[17] S. M. Foiles, M. I. Baskes, and M. S. Daw, Phys. Rev. B **33**, 7983 (1986).

[18] L. Strong and G. M. Whitesides, Langmuir **4**, 546 (1988).

[19] C. Vericat, M. E. Vela, and R. C. Salvarezza, Phys. Chem. Chem. Phys. **7**, 3258 (2005).

[20] W. L. Jorgensen, D. S. Maxwell, and J. Tirado-Rives, J. Am. Chem. Soc. **118**, 11225 (1996).

[21] H. W. Horn, W. C. Swope, J. W. Pitera, J. D. Madura, T. J. Dick, G. L. Hura, and T. Head-Gordon, J. Chem. Phys. **120**, 9665 (2004).

[22] J. L. F. Abascal and C. Vega, J. Chem. Phys. **123**, 234505 (2005).

[23] J.-P. Ryckaert, G. Ciccotti, and H. J. Berendsen, J. Comput. Phys. **23**, 327 (1977).

[24] T. Schneider and E. Stoll, Phys. Rev. B **17**, 1302 (1978).

[25] B. Yoon, W. D. Luedtke, R. N. Barnett, J. Gao, A. Desireddy, B. E. Conn, T. Bigioni, and U. Landman, Nat. Mater. **13**, 807 (2014).

[26] C. de Kruif and H. Oonk, The Journal of Chemical Thermodynamics **11**, 287 (1979).

[27] R. Hockney and J. Eastwood, *Computer Simulation Using Particles* (Taylor & Francis, 1988).

[28] M. Tuckerman, B. J. Berne, and G. J. Martyna, J. Chem. Phys. **97**, 1990 (1992).